Hybrid Control of 3D-Printed Multimodal Soft Pneumatic Actuators

Xuan Tung Le
Dept. of Mechanical Engineering
Texas A&M University
College Station, Texas, USA
tung2250@tamu.edu

P. D. S. Hiroshan Gunawardane
Dept. of Mechanical Engineering
The University of British Columbia
Vancouver, British Columbia, Canada
hiroshan@mail.ubc.ca

Sanjaya Mallikarachchi
Dept. of Multidisciplinary Engineering
Texas A&M University
College Station, Texas, USA
sanjayadpf@tamu.edu

Mu Chiao
Dept. of Mechanical Engineering
The University of British Columbia
Vancouver, British Columbia, Canada
muchiao@mech.ubc.ca

Isuru S. Godage
Dept. of Engineering Technology & Industrial Distribution
Texas A&M University
College Station, Texas, USA
igodage@tamu.edu

***Abstract*—Soft pneumatic actuators (SPAs) offer a promising alternative for biomedical applications requiring high sensitivity and precise manipulation due to their inherent compliance. 3D-printed multi-modal zig-zag SPAs exhibit potential in this area by achieving repeatable and precise shape changes due to their chambered design. However, achieving accurate position control remains a challenge. This work proposes a hybrid control strategy for multi-modal zig-zag SPAs that combines feed-forward and proportional-integral-derivative (PID) control to enhance positioning accuracy. A Pseudo Rigid Body (PRB) based inverse dynamic model is employed for the feed-forward component. The effectiveness of the controller is evaluated through extensive simulations and experiments. Results demonstrate that the hybrid control strategy achieves up to 29.5% and 31.6% improvement in accuracy compared to the PID and feed-forward controllers, respectively, within the operational bandwidth.**

***Index Terms*—Soft pneumatic actuators, Biomedical applications, Hybrid control, Position control, PRB model**

I. Introduction

Soft robotics has emerged as a valuable tool within the field of biomedical robotics and biomechatronics, particularly for applications in sensing [1] and actuation [2]. This technology offers distinct advantages due to the inherent compliance, flexibility, and adaptability of soft robots. These characteristics make them inherently human-friendly, enabling smooth interaction and improved human-machine interfaces [3], [4]. Soft pneumatic actuators (SPAs) play a central role in these designs. Their compliant nature allows robots to perform diverse tasks [5]. SPAs offer unique capabilities in flexibility and adaptability, enabling the generation of motion and forces beyond the reach of traditional electromechanical robots [6]. SPA-based systems have been successfully tested in various applications, including surgical robotics [7], rehabilitation [8], and health monitoring, demonstrating their versatility and effectiveness (see Fig. 1). Recent advancements in fully 3D-printed Zig-zag SPAs [10], [11] represents a significant leap forward in the field. These actuators offer comparatively high positioning accuracy compared to other SPA variants, such as membrane-type mold/cast SPAs and artificial muscles [12]. Conventional SPAs often suffer from inherent design inconsistencies, leading to undesirable nonlinearities that complicate real-time system modeling and control. Addressing these nonlinearities has historically proven challenging. However, the interconnected zig-zag chamber-like design structure, coupled with advanced manufacturing processes like 3D printing using Thermoplastic Polyurethane (TPU), has successfully minimized the impact of nonlinearities, particularly in lower frequency actuation [11]. Another significant challenge in SPAs involves maintaining force output while achieving high flexibility, due to the inherently low mechanical stiffness of polymers. TPU-based 3D-printed SPAs have demonstrated the ability to overcome this challenge through strategic designs that incorporate seamless structures with stiffer materials compared to conventional

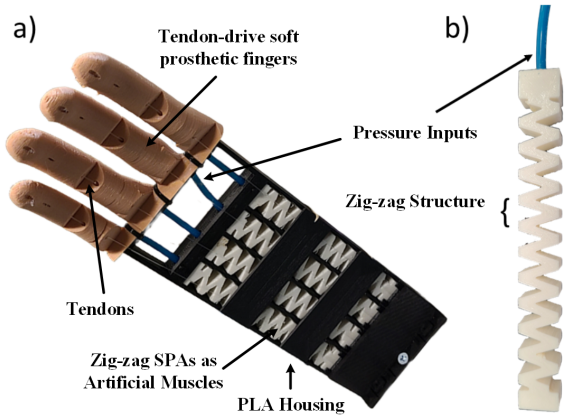

Fig. 1: A test prototype of a platform for tendon-driven soft prosthetic hands [9] controlled using zig-zag SPAs. [a]. Prosthetic hand test platform that uses zig-zag SPAs [10]. [b]. 3D-printed linear zig-zag SPAs.

polymers [13]. The Zig-zag SPA is a noteworthy example of a multi-modal actuator, offering linear motion with enhanced flexibility and increased output force. This makes it suitable for a wide range of applications [1], [10].

Researchers have explored various control strategies for SPAs, categorized as model-based, model-free, and hybrid approaches [14]. Hybrid controllers offer a comprehensive strategy by combining elements of both model-based and model-free techniques [14]. While model-based controllers provide valuable insights into system dynamics, solely relying on model-free approaches might not be optimal for SPA control. Kinematic and dynamic model-based controllers have been proposed for SPAs. For instance, [15] introduces a variable curvature continuum kinematic model. However, this approach relies on linear approximations of kinematics, which can lead to significant tracking errors, especially for large movements within a control loop cycle. Additionally, these methods neglect dynamic interactions between robot joints, such as inertial forces and torques, which become crucial at higher speeds. Another approach employs a cascaded PI-PID control strategy based on a kinematic model [16]. Similar to the previous example, kinematic-based strategies suffer from the limitation of precise control due to the absence of dynamic interactions. To address this, researchers have proposed control strategies that incorporate dynamic models. A controller combining feed-forward control, feedback linearization, and linear control techniques to manage nonlinearities was presented in [17]. Similarly, [18] introduced a control strategy combining a PD controller and feedback linearization. While these strategies address dynamic interactions, the complexity of the dynamic model can lead to reduced precision at high speeds. The approach presented in [19] aims to overcome precision limitations associated with high speeds and complex dynamic models. This approach incorporates a dynamic model based on beam theory, offering a balance between model complexity and control effectiveness.

This paper presents a real-time controller designed for zig-zag SPAs suited for higher positional accuracy. The proposed method leverages a hybrid control approach, combining an inverse dynamics model as a feed-forward controller with a PID feedback controller compensating the unattainable errors by the inverse dynamic model. The paper is structured as follows. Sec. II-A details the fabrication process of the SPA and Pseudo Rigid Body (PRB) model. Sec. III focuses into the complexities of the controller design and the underlying control strategy. Sec. IV presents the experimental results and validates the effectiveness of the proposed controller. Lastly, Sec. V provides a comprehensive discussion, offering insights and conclusions derived from this study.

II. Actuator System Model

A. Zig-zag Soft Pneumatic Actuator

The spring-like structure of the zig-zag SPA (Fig. 1b), characterized by a uniform cross-sectional area, linearly expands upon pressurization, achieving a 30% extension at approximately 350 kPa and generating a 9.34 N blocking force.

TABLE I: The design parameters and comprehensive specifications of the fabricated linear extension multimodal zig-zag SPA.

Parameter	Value
Length(L)	134 mm
Width(W)	16 mm
Height(H)	13 mm
Wall thickness [chambers] (t)	0.6 mm
Chamber angle (α)	45°
Pressure range (δP)	0-350 kPa
Extension range (δL)	0-40 mm
Strain-limiting-layer thickness (s)	0.5 mm
Mass(m)	13 g
Bending angle range ($\delta\theta$)	0-100°

Designed using SolidWorks 2023, the zig-zag SPA actuator underwent 3D printing preparations with Simplify3D and Flash Print 5 software. The Flash Forge Dreamer NX 3D printer, configured as specified in [20], [21], executed the 3D printing process. Ninja Flex Snow (diameter of 1.75 mm and a hardness 95A TPU), served as the printing material. Air tubes for air supply were integrated into structural components through small apertures. The design specifications for the zig-zag SPA prototype are detailed in Table I. Detailed information of the design, fabrication, and static characterization of the SPA can be found in [10] and [11].

B. Forward and Inverse Dynamic Models

The Zig-zag SPA is modeled using the PRB approach incorporating dynamics lacking in kinematic models [22], [23]. The model is built by utilizing the MATLAB Simulink Simscape (see Fig. 2). This approach provides an efficient dynamic model without compromising the structure of the actuator that can be effectively used in developing a real-time controller. The governing equation of motions of the PRB dynamic model is represented as follows in standard notation $q \in \mathbb{R}$ representing the angular position and $\tau_{input} \in \mathbb{R}$ representing the joint torque.

$$M(q)\ddot{q} + C(q,\dot{q})\dot{q} + G(q) = \tau_{input} \tag{1}$$

The torque sequence variation as illustrated in Fig. 2 for the expansion behavior can be depicted as follows

$$\tau_{input} = \begin{bmatrix} \tau_1 & -\tau_2 & \tau_3 & -\tau_4 & \dots & \tau_n \end{bmatrix}^T \tag{2}$$

The inverse model is obtained using the forward Simscape model by changing the model to be driven by angular position input which then computes the required torque. Then it is used as the feed-forward controller input described in Sec. III. To map the the input pressure to the prototype SPA with the corresponding torque input of the forward dynamic model we utilized MATLAB *fmincon* function to minimize the tip position error upon forward actuation to obtain the pressure vs torque relationship described in [11]. The angular joint stiffness values used for expansion $1.3296\,\mathrm{N\,m\,rad^{-1}}$ were obtained using an experimental procedure.

C. Stiffness Estimation

The procedure of stiffness calculation involves hanging a known mass of 50 g and measuring the resulting overall

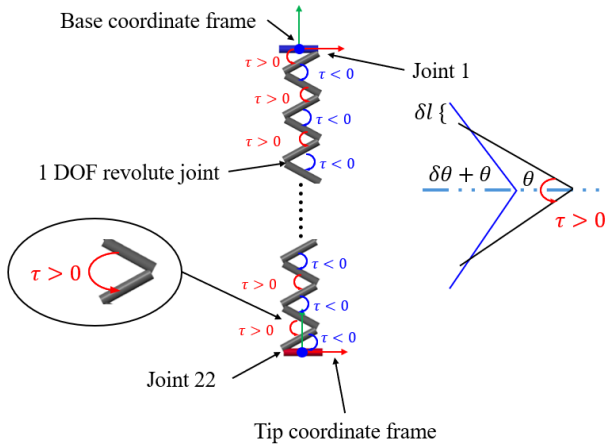

Fig. 2: PRB Model illustrated in MATLAB Simscape. Blue and red τ values depict applied pressure effects that enable linear expansion. The adjacent diagram illustrates the geometry of a revolute joint under torque.

extension to calculate linear stiffness (k_l). Then, we calculate the extension contributed by the rotation of each rigid segment, denoted as δl, within the structure. The total number of these rigid segments is denoted as n. Using Hooke's Law, we determine the total force F generated by the known mass. We calculate the torque acting on each segment due to the applied weight, with d representing the length of an individual rigid cylindrical element in the rigid-body model. The extension is denoted as δl caused by the rotation of each segment as described in (3), where θ_0 represents the initial angle of the actuator.

$$\delta l = d\sin(\theta_0 + \delta\theta) - d\sin\theta_0 \tag{3}$$

Considering the rotational stiffness k_θ, we can derive the torque as shown in (4) based on the geometric configuration shown in Fig. 2 as,

$$k_\theta = \frac{Fd}{2\left[\sin^{-1}\left(\frac{F}{dnk_l} + \sin\theta_0\right) - \theta_0\right]} \tag{4}$$

Once the k_θ is determined the pressure and torque relationship is obtained utilizing MATLAB *fmincon* function using the forward PRB model converging to the experimental displacement. Both the forward and inverse model assumes identical torque and position for all the joints in the PRB model. We obtain the average of all the torques computed from the inverse model using the given position inputs for the feed-forward controller.

III. Controller Design

A. Hybrid Control Strategy

We utilize a combination of feed-forward and proportional-integral-derivative (PID) control to regulate the SPA. We tune the contributions of individual controllers for the optimal controller performance. The feed-forward controller provide the initial input for the actuator. However, it is important to note that the inverse dynamic model may not fully account for certain real-world factors associated with the actuator. As a result, discrepancies between the model and reality can lead to errors, which are subsequently addressed through the use of a PID controller with a feedback loop. Fig. 3 shows the main control schematic of the system.

B. Controller Strategy Analysis

The robustness of the controller is assessed through analysis before implementing it on the physical prototype. This analysis focuses on evaluating the significance of individual control components and their contributions to achieving precise position control for our expansion SPA. Initially, we conducted simulation experiments employing the PRB dynamic model as the surrogate plant. These experiments involved introducing transport delays and random noise to assess the controller's resilience. Subsequently, we examined the effectiveness of each controller in three distinct scenarios: Feed-forward control alone, PID control alone, and a Hybrid controller combining both approaches. Based on the simulation data, we tested an actual SPA prototype to validate the findings and performance of the controller in a real-world context.

C. Simulation Results

We perform the simulation utilizing the PRB dynamic model to understand the contribution of each control component in the hybrid control strategy. Then we test the controller providing sinusoid input signals with frequencies of 0.2 Hz, 0.4 Hz, and 1 Hz. To incorporate real-world conditions, we added noise of 0.6 mm as similar to the noise observed from the camera feedback. The feedback had a delay of 0.05 s and was sampled at 30 Hz to represent the real-world condition. Finally, the input to the forward PRB dynamic model was limited from 0 to 0.6 N m corresponding to 0 to 3.5 bar pressure input to the real-life actuator. Fig. 4 shows how each control component contributes to the position control of the hybrid controller and the error of each controller in the simulation. To examine the improvement using the hybrid controller, we compared the RMSE, mean error, and maximum error in 5 oscillation cycles of the reference signal. Note here that the maximum error was only examined after 20 seconds as this was when all the controllers were stable and each controller's performance could be compared. The simulation study RMSE, mean error, and maximum error values are depicted in Table II. All types of error in the actuator are measured in millimeters (*mm*). The table shows that when the reference signal has a high frequency, the hybrid controller shows better performance than other controllers. The hybrid controller can achieve an RMSE, mean error, and maximum error as small as 0.3 mm, 0.3 mm, and 0.9 mm, respectively. Table II also shows the percentage improvement of the hybrid controller. Based on the table, the hybrid controller can reduce error up to 44.5% for RMSE, 47.6% for mean error, and 33.2% for maximum error.

IV. Experimental Results

A. Testing Setup

The setup for the robot experiment is illustrated in Fig. 3. Air pressure is sourced from an 8-bar compressor and

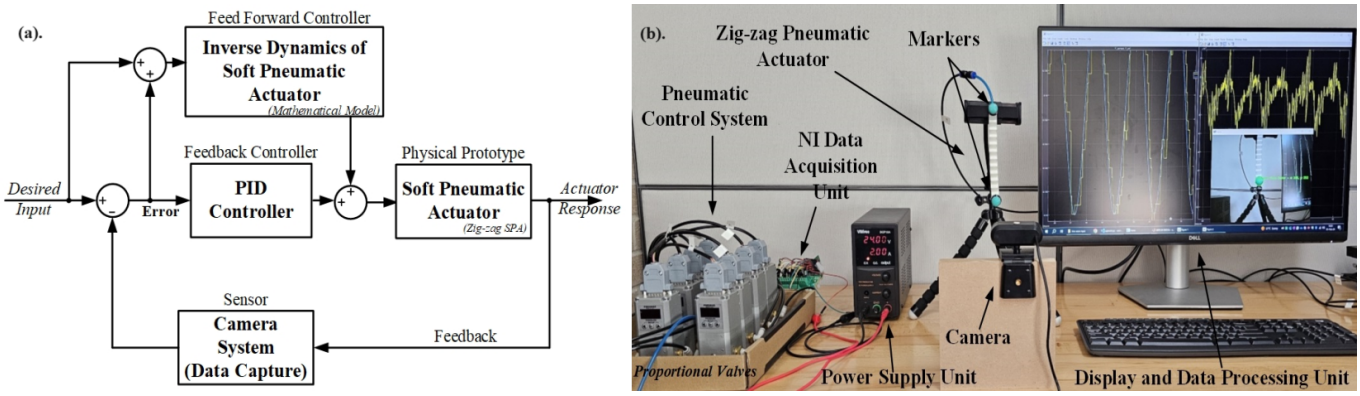

Fig. 3: Schematic diagram and the experimental setup. (a). The schematic diagram of the real-time controller for the Zig-zag SPA. A PID feedback controller is employed to address errors within the camera-based feedback loop. Subsequently, the inverse dynamics of the SPA are integrated into the controller using the feed-forward method as illustrated. (b). Experimental setup. The SPA position was controlled through proportional valves using the camera feedback and model-based feed-forward control system.

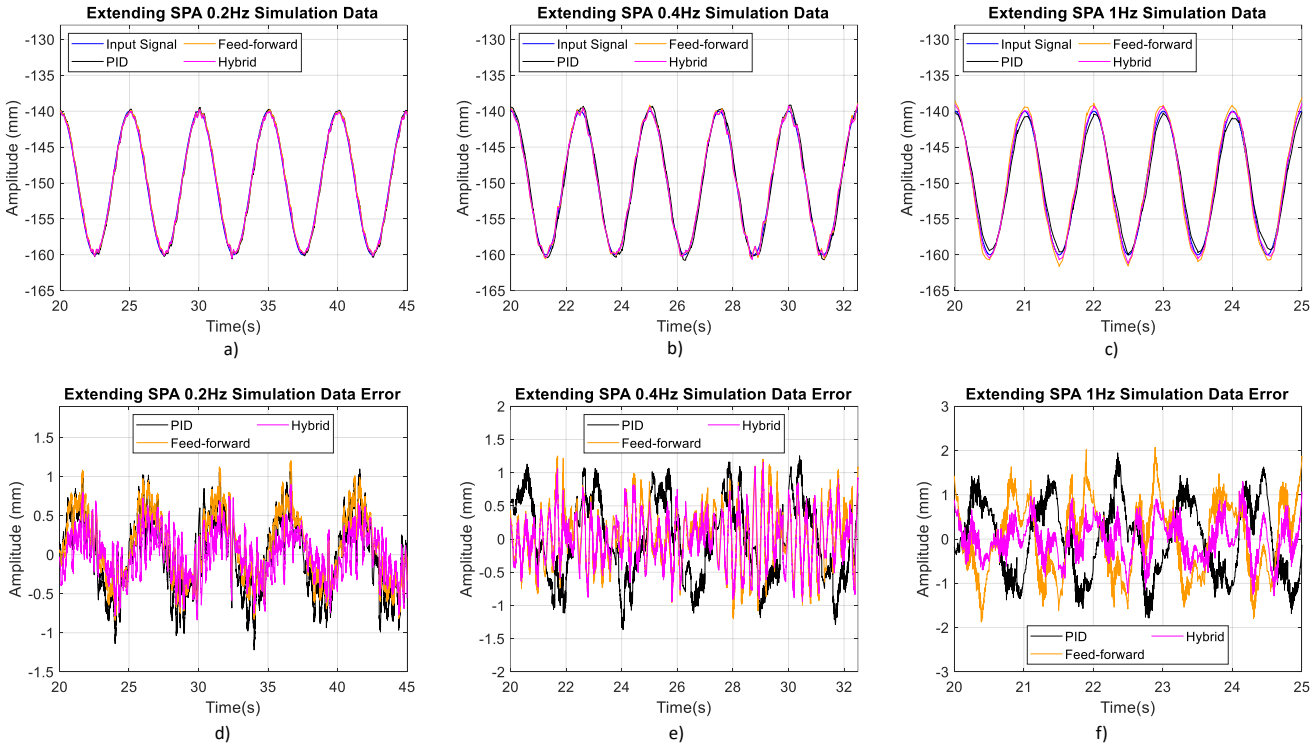

Fig. 4: Simulation controller response and error for input frequencies of 0.2 Hz, 0.4 Hz, 1 Hz.

applied to SPA using a digital proportional pressure regulator (Pneumax, 171E2N.T.D.0009, ITALY), as shown in Fig. 3B. The pressure regulator is interfaced with MATLAB Simulink Desktop Real-Time model via a data acquisition card (PCI-6703, NI USA), which transmits an analog voltage signal ranging from 0 to 10 V that is mapped to a pressure ranging from 0 to 3.5 bar. The mapping equation is $P = \frac{3.5V}{10}$, where P is the pressure in bar and V represents the voltage. To control the SPAs, a 30 Hz camera-based position tracker was used to track the tip position of the SPA and provide feedback to the controller via a UDP server in MATLAB Simulink.

B. Controller Evaluation

Experiments for the extending prototype SPA. Fig. 5 shows how the actuator responded to each type of controller and the controllers' error with input frequencies of 0.2 Hz, 0.4 Hz, and 1 Hz in the experiment. Table III shows the RMSE, mean error, and maximum error when using each type of controller with input frequencies of 0.2 Hz, 0.4 Hz, and 1 Hz. Further, we conduct step response experiments for all three types of controllers as shown in Fig. 6.

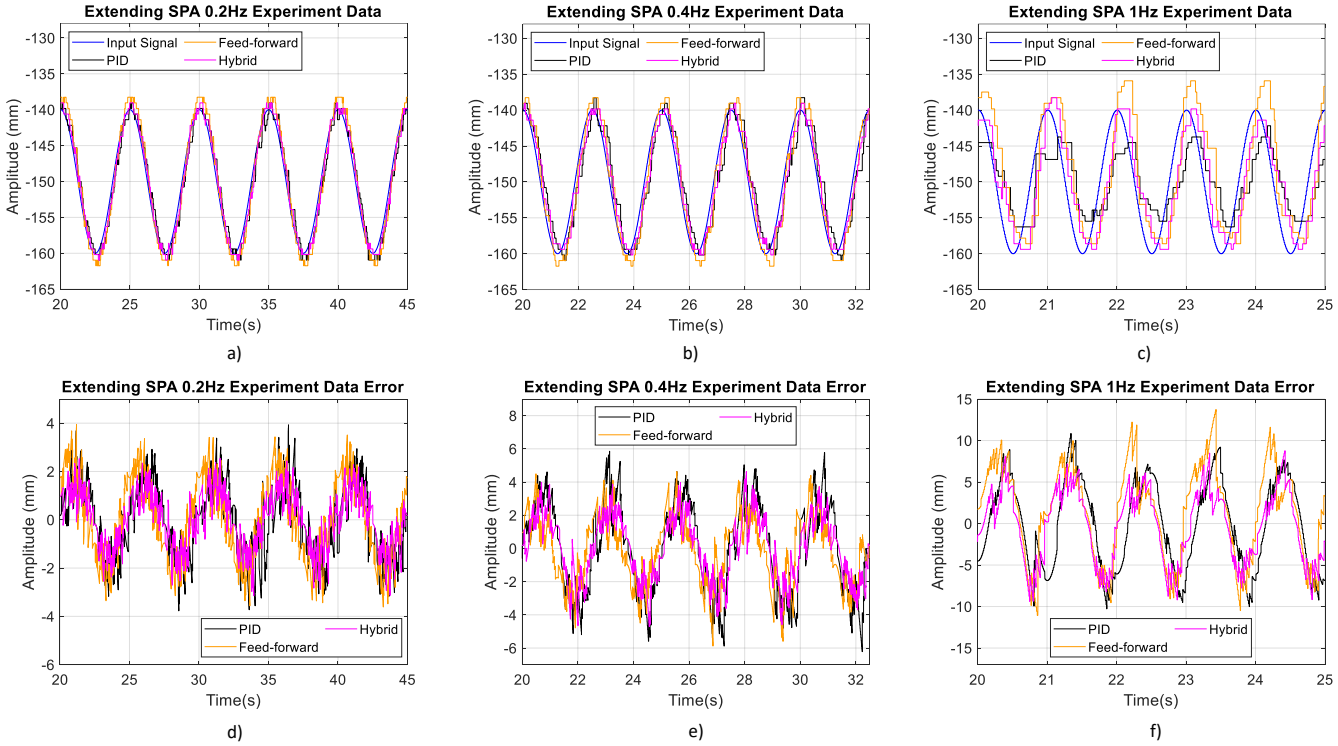

Fig. 5: Experiment controller response and error for input frequencies of 0.2 Hz, 0.4 Hz, 1 Hz.

TABLE II: SPA control simulation data | mm (% improvement when using Hybrid controller instead)

Signal frequency (Hz)	RMSE (mm) (%)			Mean error (mm) (%)			Maximum error (mm) (%)		
	Hybrid	Feed Forward	PID	Hybrid	Feed Forward	PID	Hybrid	Feed Forward	PID
0.2 Hz	0.3	0.5 (32.8%)	0.5 (37.8%)	0.3	0.4 (32.3%)	0.5(40.1%)	0.9	1.2 (25.4%)	1.2(26.3%)
0.4 Hz	0.4	0.5 (12.0%)	0.7 (40.1%)	0.3	0.4 (15.3%)	0.6 (43.3%)	1.1	1.2 (8.7%)	1.4 (19.5%)
1 Hz	0.5	0.8 (34.4%)	0.9 (44.5%)	0.4	0.7 (37.3%)	0.8(47.6%)	1.3	1.9 (31.1%)	1.9 (33.2%)

TABLE III: SPA control experiment data | mm (% improvement when using Hybrid controller instead)

Signal frequency (Hz)	RMSE (mm) (%)			Mean error (mm) (%)			Maximum error (mm) (%)		
	Hybrid	Feed Forward	PID	Hybrid	Feed Forward	PID	Hybrid	Feed Forward	PID
0.2 Hz	1.1	1.7 (31.6%)	1.5 (24.6%)	1.0	1.5 (32.9%)	1.3 (25.4%)	3.1	3.9 (21.1%)	3.9 (20.4%)
0.4 Hz	1.9	2.1 (8.0%)	2.7 (29.5%)	1.7	1.8 (6.7%)	2.4 (30.3%)	4.7	5.7 (17.8%)	6.1 (23.3%)
1 Hz	4.4	5.9 (25.2%)	5.4 (18.6%)	3.8	5.1 (25.6%)	4.8 (20.6%)	9.4	13.6 (30.9%)	10.8 (13.2%)

C. Discussion

Our experiment results agree with the simulation and the hybrid controller has lower error values compared to the feed-forward controller and PID controller. Fig. 5 also shows that in 0.2 Hz and 0.4 Hz, feed-forward and PID controllers alone are still able to track the reference signal. However, with a reference sinusoid signal of 1 Hz frequency, both of them struggle to track the reference signal. They are either not fast enough (PID alone) or have a lot of overshoot (feed-forward alone) while the hybrid controller is still able to track the reference signal. In table III, the hybrid controller reduces the error up to 31.6% for RMSE, 32.9% for mean error, and 30.9% for maximum error. These results show that the controller that combines feed-forward and PID controllers can improve the control performance significantly, especially for high-frequency reference signals. For the step-input experiment results in Fig. 6, all the controllers follow the input with minor oscillations evidencing that controllers are stable.

V. Conclusions

In this work, we utilized 3D-printed Multimodal zig-zag SPA that has a spring-like structure that can expand linearly due to provided air pressure. The chamber-like structure of the actuator allows it to have repeatable precise shape deformation which shows its potential in biomedical applications such as prosthetic prototypes shown in Fig. 1. To control the SPA, we designed a hybrid controller based on the PRB model we proposed in [11]. This hybrid controller combines PID and feed-forward controllers utilizing the PRB inverse dynamic model of the SPA. The simulation study demonstrated that the hybrid approach outperforms feedback controllers for highly nonlinear zig-zag SPAs. The proposed control strategy achieved the reduction of RMSE, mean error, and maximum

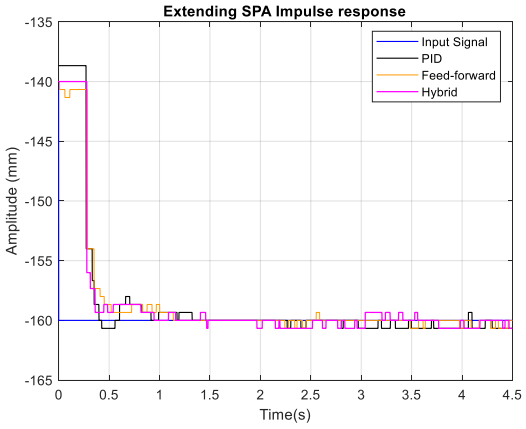

Fig. 6: Experiment step response

error up to 31.6%, 32.9%, and 30.9% respectively. Future work will incorporate hysteresis and nonlinear effects for improved performance and explore multi-degree-of-freedom manipulators.

ACKNOWLEDGMENT

The authors express their sincere gratitude for the funding sources that have generously supported this research; The Friedman Award for Scholars in Health at UBC, and the NSERC CREATE grant (565429-2022). This work was supported also in part by the National Science Foundation (NSF) grants IIS-2325491(2008797), CMMI-2326536(2048142), CMMI-2327702(2132994) and National Institute of Health (NIH) R01 grant 5R01NS116148-04.

REFERENCES

[1] Y. Ye, Z. Wan, P. Gunawardane, Q. Hua, S. Wang, J. Zhu, M. Chiao, S. Renneckar, O. J. Rojas, and F. Jiang, "Ultra-stretchable and environmentally resilient hydrogels via sugaring-out strategy for soft robotics sensing," *Advanced Functional Materials*, p. 2315184, 2024.

[2] S. Ham, B. B. Kang, J. Kim, S. Hwang, and W. Kim, "Development of soft variable stiffness actuator with tendon-driven layer jamming mechanism," in *2022 9th IEEE RAS/EMBS International Conference for Biomedical Robotics and Biomechatronics (BioRob)*. IEEE, 2022, pp. 1–6.

[3] P. Gunawardane, N. Budiardjo, G. Alici, C. De Silva, and M. Chiao, "Thermoelastic strain-limiting layers to actively-control soft actuator trajectories," in *2022 IEEE 5th International Conference on Soft Robotics (RoboSoft)*. IEEE, 2022, pp. 48–53.

[4] L. De Arco, O. Ramos, M. Múnera, M. Moazen, H. Wurdemann, and C. A. Cifuentes, "The prhand: Functional assessment of an underactuated soft-robotic prosthetic hand," in *2022 9th IEEE RAS/EMBS International Conference for Biomedical Robotics and Biomechatronics (BioRob)*. IEEE, 2022, pp. 1–6.

[5] P. D. S. H. Gunawardane, R. E. A. Pallewela, and N. T. Medagedara, "Tele-operable controlling system for hand gesture controlled soft robot actuator," in *2019 2nd IEEE International Conference on Soft Robotics (RoboSoft)*. IEEE, 2019, pp. 656–662.

[6] U. Gupta, L. Qin, Y. Wang, H. Godaba, and J. Zhu, "Soft robots based on dielectric elastomer actuators: A review," *Smart Materials and Structures*, vol. 28, no. 10, p. 103002, 2019.

[7] H. Abidi, G. Gerboni, M. Brancadoro, J. Fras, A. Diodato, M. Cianchetti, H. Wurdemann, K. Althoefer, and A. Menciassi, "Highly dexterous 2-module soft robot for intra-organ navigation in minimally invasive surgery," *The International Journal of Medical Robotics and Computer Assisted Surgery*, vol. 14, no. 1, p. e1875, 2018.

[8] P. Polygerinos, Z. Wang, K. C. Galloway, R. J. Wood, and C. J. Walsh, "Soft robotic glove for combined assistance and at-home rehabilitation," *Robotics and Autonomous Systems*, vol. 73, pp. 135–143, 2015.

[9] R. Abayasiri, R. Abayasiri, R. Gunawardhana, R. Premakumara, S. Mallikarachchi, R. Gopura, T. D. Lalitharatne, and D. Madusanka, "An under-actuated hand prosthesis with finger abduction and adduction for human like grasps," in *2020 6th International Conference on Control, Automation and Robotics (ICCAR)*. IEEE, 2020, pp. 574–580.

[10] P. D. S. H. Gunawardane, P. Cheung, H. Zhou, G. Alici, C. W. de Silva, and M. Chiao, "A versatile 3d-printable soft pneumatic actuator design for multi-functional applications in soft robotics," *Soft Robotics*, 2024.

[11] S. Mallikarachchi, P. H. Gunawardane, X. T. Le, M. Chiao, and I. S. Godage, "Multimodal soft robotic actuator modeling and validation," in *2024 IEEE 7th International Conference on Soft Robotics (RoboSoft)*. IEEE, 2024, pp. 359–365.

[12] D. D. Arachchige *et al.*, "Soft steps: Exploring quadrupedal locomotion with modular soft robots," *IEEE Access*, vol. 11, pp. 63 136–63 148, 2023.

[13] J. D. Hubbard, R. Acevedo, K. M. Edwards, A. T. Alsharhan, Z. Wen, J. Landry, K. Wang, S. Schaffer, and R. D. Sochol, "Fully 3d-printed soft robots with integrated fluidic circuitry," *Science Advances*, vol. 7, no. 29, p. eabe5257, 2021.

[14] T. George Thuruthel, Y. Ansari, E. Falotico, and C. Laschi, "Control strategies for soft robotic manipulators: A survey," *Soft robotics*, vol. 5, no. 2, pp. 149–163, 2018.

[15] T. Mahl, A. Hildebrandt, and O. Sawodny, "A variable curvature continuum kinematics for kinematic control of the bionic handling assistant," *IEEE transactions on robotics*, vol. 30, no. 4, pp. 935–949, 2014.

[16] A. D. Marchese and D. Rus, "Design, kinematics, and control of a soft spatial fluidic elastomer manipulator," *The International Journal of Robotics Research*, vol. 35, no. 7, pp. 840–869, 2016.

[17] V. Falkenhahn, A. Hildebrandt, R. Neumann, and O. Sawodny, "Dynamic control of the bionic handling assistant," *IEEE/ASME Transactions on Mechatronics*, vol. 22, no. 1, pp. 6–17, 2016.

[18] A. D. Kapadia, K. E. Fry, and I. D. Walker, "Empirical investigation of closed-loop control of extensible continuum manipulators," in *2014 IEEE/RSJ International Conference on Intelligent Robots and Systems*. IEEE, 2014, pp. 329–335.

[19] W.-T. Yang, B. Kürkçü, M. Hirao, L. Sun, X. Zhu, Z. Zhang, G. X. Gu, and M. Tomizuka, "Control of soft pneumatic actuators with approximated dynamical modeling," in *2023 IEEE International Conference on Robotics and Biomimetics (ROBIO)*. IEEE, 2023, pp. 1–8.

[20] C. Tawk, G. M. Spinks, M. in het Panhuis, and G. Alici, "3d printable linear soft vacuum actuators: their modeling, performance quantification and application in soft robotic systems," *IEEE/ASME Transactions on Mechatronics*, vol. 24, no. 5, pp. 2118–2129, 2019.

[21] C. Tawk, M. in het Panhuis, G. M. Spinks, and G. Alici, "Bioinspired 3d printable soft vacuum actuators for locomotion robots, grippers and artificial muscles," *Soft robotics*, vol. 5, no. 6, pp. 685–694, 2018.

[22] D. D. Arachchige, D. M. Perera, S. Mallikarachchi, I. Kanj, Y. Chen, and I. S. Godage, "Wheelless soft robotic snake locomotion: Study on sidewinding and helical rolling gaits," in *2023 IEEE International Conference on Soft Robotics (RoboSoft)*. IEEE, 2023, pp. 1–6.

[23] D. M. Perera, D. D. Arachchige, S. Mallikarachchi, T. Ghafoor, I. Kanj, Y. Chen, and I. S. Godage, "Teleoperation of soft modular robots: Study on real-time stability and gait control," in *IEEE Int. Conf. on Soft Robotics (RoboSoft)*, 2023, pp. 01–07.